

Insights into the structural dynamics, thermophysical properties, and thermodynamics of the NaCl-ThCl $_{\!_{A}}$ and NaCl-UCl $_{\!_{A}}$ systems

ter Veer, N. T.H.; de Vries, W. K.; Heyning, C. T.C.; Abbink, T. F.; Ocádiz-Flores, J. A.; Gheribi, A. E.; Konings, R. J.M.; Smith, A. L.

DOI

10.1016/j.mollig.2025.128590

Publication date 2025

Document VersionFinal published version

Published in Journal of Molecular Liquids

Citation (APA)

ter Veer, N. T. H., de Vries, W. K., Heyning, C. T. C., Abbink, T. F., Ocádiz-Flores, J. A., Gheribi, A. E., Konings, R. J. M., & Smith, A. L. (2025). Insights into the structural dynamics, thermophysical properties, and thermodynamics of the NaCl-ThCl_and NaCl-UCl_systems. *Journal of Molecular Liquids*, *437*, Article 128590. https://doi.org/10.1016/j.molliq⁴.2025.128590 4

Important note

To cite this publication, please use the final published version (if applicable). Please check the document version above.

Copyright

Other than for strictly personal use, it is not permitted to download, forward or distribute the text or part of it, without the consent of the author(s) and/or copyright holder(s), unless the work is under an open content license such as Creative Commons.

Takedown policy

Please contact us and provide details if you believe this document breaches copyrights. We will remove access to the work immediately and investigate your claim.

ELSEVIER

Contents lists available at ScienceDirect

Journal of Molecular Liquids

journal homepage: www.elsevier.com/locate/molliq



Insights into the structural dynamics, thermophysical properties, and thermodynamics of the NaCl-ThCl₄ and NaCl-UCl₄ systems

N.T.H. ter Veer^a, W.K. de Vries^a, C.T.C. Heyning^a, T.F. Abbink^a, J.A. Ocádiz-Flores^a, A.E. Gheribi b, R.J.M. Konings^a, A.L. Smith^{a,*}

a Radiation Science & Technology Department, Faculty of Applied Sciences, Delft University of Technology, Mekelweg 15, Delft, 2629 JB, the Netherlands

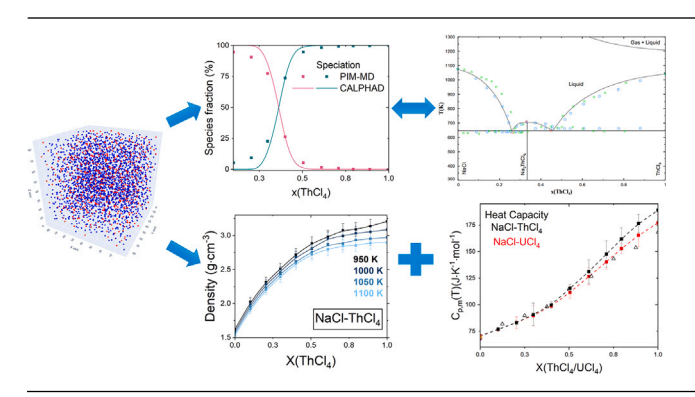
HIGHLIGHTS

- New polarisable ion model (PIM-MD) force fields were developed for ThCl₄ and UCl₄.
- Structural and thermophysical properties of molten ThCl₄ and UCl₄ were elucidated.
- NaCl-AnCl₄ (An = Th, U) mixtures were investigated using PIM-MD.
- Thermodynamic models of NaCl-AnCl₄
 (An = Th, U) are reported.
- The models couple MD-derived chemical speciation with phase equilibria.

ARTICLE INFO

Keywords:
Molten salts
ThCl₄
UCl₄
Molecular dynamics
CALPHAD

GRAPHICAL ABSTRACT



ABSTRACT

The structural, thermochemical, and thermophysical properties of the $AnCl_4$, and $NaCl-AnCl_4$ (An = Th, U) melts were investigated using molecular dynamics (MD) simulations based on the Polarisable Ion Model (PIM). New force fields were proposed and used to compute key properties including density, thermal expansion, enthalpy of mixing, heat capacity, as well as the local structure and chemical speciation in the molten (Na, An) Cl_x (An = Th, U) salts. Thermodynamic models were then developed based on the CALPHAD method, using both PIM-MD and experimental data as input. Employing the modified quasichemical formalism in the quadruplet approximation for the liquid solution, the models account for the chemical speciation in the melt as calculated by MD simulations, and reproduce well phase equilibria in those systems. In particular, the models included monomeric and dimeric species to represent the physical nature of the ionic melt, which shows progressive oligomerisation with increasing $AnCl_4$ fraction. Our studies confirm that the melt becomes highly volatile at high $AnCl_4$ fractions, which is discussed in light of the results obtained herein.

b Concordia University, Department of Chemical and Materials Engineering (CME), Montreal, H3G 2W1, Quebec, Canada

Corresponding author.
 Email address: a.l.smith@tudelft.nl (A.L. Smith).

1. Introduction

The Molten salt reactor (MSR) is a type of nuclear fission system in which the primary coolant and fuel consist of molten fluorides or chlorides. These reactors offer promising advancements in nuclear energy technology due to the use of a liquid fuel with high thermal conductivity and low melting point, which enhances reactor efficiency and operational flexibility [1]. Historically, there has been significant research and interest in fluoride salts, which have been extensively studied [2]. However, there has been a notable surge in research endeavours focused on chloride MSRs in recent years [3], particularly suited for a fast spectrum reactor. Exploring their potential presents a significant avenue for innovation and development in pursuing safe, efficient, and sustainable energy solutions. Examples of chloride fuel salts that have been investigated include NaCl-PuCl₃ [4], NaCl-UCl₃-PuCl₃ [5], NaCl-MgCl₂-PuCl₃ [6], and the promising fuel salt mixture NaCl-ThCl₄-PuCl₃ [71.

The NaCl-ThCl $_4$ -PuCl $_3$ fuel salt is considered particularly promising because of the possibility it offers for implementing thorium breeding in molten salt fast reactors, while simultaneously enabling plutonium burning from current civilian and military stockpiles [7]. Thorium moreover offers two major benefits in a nuclear fuel cycle: it is highly abundant in the Earth's crust [8], providing a potentially more sustainable fuel source for nuclear energy production than uranium; and secondly, thorium-based fuel cycles have the potential to generate less long-lived transuranic waste, thus contributing to reduced environmental impact and improved safety [9]. Thorium in nature is found as the isotope 232 Th, which is fertile. 232 Th will undergo successive neutron captures and beta decays in a nuclear reactor, yielding fissile 233 U. Thus, for a thorium-based fuel cycle in chloride molten salt reactors, UCl $_4$ based systems are equally important.

This study focuses on the thermochemical and thermophysical properties of ${\rm AnCl_4}$ and ${\rm NaCl\text{-}AnCl_4}$ (An = Th, U) systems, through a combination of computational methods, with the aim of gaining an enhanced understanding of the relationship between the salt properties and structural behaviour across a broad range of temperatures and compositions. The density, thermal expansion, mixing enthalpy, heat capacity, and chemical speciation of pure ${\rm AnCl_4}$ and ${\rm NaCl\text{-}AnCl_4}$ (An = Th, U) mixtures have been computed using Polarisable Ion Model-Molecular Dynamics (PIM-MD) simulations, and compared to literature data when available.

In addition, the gas-phase thermodynamic properties of pure UCl_4 and $ThCl_4$ have been critically reassessed and reoptimised based on a comprehensive review of the literature, allowing for a complete description of solid, liquid, and vapour phases in NaCl-AnCl $_4$.

It is important to mention that various force fields and computational methods including Ab Initio Molecular Dynamics (AI-MD), Density Functional Theory (DFT), and Machine Learning (ML) potentials for molten salts are reported in the literature, often showing significant discrepancies between different approaches [10,11]. This work examines the impact of fine-tuning the PIM-MD interaction potentials using the repulsion parameters, particularly in light of density data. One of the key motivations for looking at this is the discrepancy noticed in the literature with respect to the density of ThCl₄ and UCl₄ [12–15]. A particularly perplexing observation is that Kuroda et al. [12] reported density of pure ThCl₄ to be higher than that of UCl₄ (or molar volumes of pure ThCl₄ to be lower than UCl₄), which contradicts expectations considering the ionic radius contraction along the series of actinide elements, as well as data from various sources.

Recent thermodynamic models of NaCl-ThCl $_4$ and NaCl-UCl $_4$ from the literature have been reported based on the quasi-chemical formalism in the quadruplet approximation [16,17]. Although widely applied to molten salt systems [18], this formalism cannot account for the complexity of the structure of the melt, which forms $[AnCl_n]^{m-}$ complexes, but also dimers, trimers, and higher polymeric chains upon increasing $AnCl_4$

concentration. We propose here to go one step further in the modelling of the salt systems, by incorporating the structural information derived from the MD simulations, following the methodology recently applied to similar systems [19–22].

2. Computational methods

2.1. Molecular dynamics

Molecular dynamics is a widespread computational tool that has proven exceptionally powerful in modelling the properties of ionic liquids. In this work, the Polarisable Ion Model (PIM-MD) was used, which has been proven to be very robust in simulating specifically molten salts [19,20]. The interatomic potentials in the PIM-MD approach include four terms:

$$V_{Total} = V_{Coulombic} + V_{Repulsion} + V_{Dispersion} + V_{Polarisation}$$
 (1)

This first term, $V_{Coulombic}(r_{ij})$ accounts for the Coulombic charge-charge interactions between ions, where q_i and q_j are the charges of ions i and ion j separated by a distance r_{ij} [23]

$$V_{Coulombic}(r_{ij}) = \sum_{i < j} \frac{q_i q_j}{r_{ij}}$$
 (2)

The second term, $V_{Repulsion}(r_{ij})$, accounts for the short-range interaction that occurs when the electron clouds of two neighbouring ions overlap. This interaction has two adjustable parameters, A_{ij} and a_{ij} [23].

$$V_{Repulsion}(r_{ij}) = \sum_{i < j} A^{ij} e^{-a^{ij}r^{ij}}$$
(3)

The third term, $V_{Dispersion}(r_{ij})$, accounts for electron fluctuations [23], leading to the formation of momentary electric fields. These fields, in turn, influence neighbouring atoms and molecules, prompting them to adapt the spatial configuration of their electrons.

$$V_{Dispersion}(r_{ij}) = -\sum_{i \le j} \left(f_6^{ij} \frac{C_6^{ij}}{(r^{ij})^6} + f_8^{ij}(r^{ij}) \frac{C_8^{ij}}{(r^{ij})^8} \right)$$
(4)

Here the strength of the dispersion interaction is characterised by two variables, C_6^{ij} for dipole-dipole dispersion and C_8^{ij} for dipole-quadrupole [23]. To correct for the short-range energy penetration effects of both the dipole-dipole and dipole-quadrupole interactions, Tang-Toennies function f_6^{ij} and f_8^{ij} are introduced [24]. This is described in Eq. (5) where b_{ij} determines the range of the damping effects:

$$f_n^{ij} = 1 - e^{b_{ij}^n r_{ij}} \sum_{k=0}^n \frac{(b_{ij}^n r_{ij})^k}{k!}$$
 (5)

The final term in Eq. (1), $V_{Polarisation}(r_{ij})$, refers to the dynamic response of a molecule's electronic charge distribution to its local environment, including the presence of nearby molecules, external electric fields, and other perturbations. Polarisation effects become significant when simulating systems involving polar or charged molecules, interactions with electric fields, and situations where the electron cloud rearrangements play a significant role. This is especially important for simulating molten salts.

$$V_{Polarisation}(r_{ij}) = \sum_{i < j} (g_d^{ij})(r^{ij}) q^i \mu_\alpha^j - g_D^{ij}(r^{ij} q^j \mu_\alpha^i) T_\alpha^{(1)} - \mu_\alpha^i \mu_\beta^j T_{\alpha\beta}^{(2)} + \sum_i \frac{1}{2\alpha^i} \left| \mu^i \right|^2 \ \ (6)$$

In this equation $T_{\alpha}^{(1)}$ is the charge-dipole interaction tensor, $T_{\alpha\beta}^{(2)}$ is the dipole-dipole interaction tensor, α_i the polarisability of ion i and its induced dipole μ_i . As for $V_{Dispersion}(r_{ij})$, a Tang-Toennies function is introduced to correct for the short-range energy penetration of

Table 1 Overview of interaction potential parameters. The values are given in atomic units, lengths in Bohr radii (1 Bohr = 0.052918 nm) and energy in Hartree (1 $E_H = 4.3597 \cdot 10^{-18}$ J).

Ion Pair	A^{ij}	a^{ij}	C_6^{ij}	C_8^{ij}	b_6^{ij}	b_8^{ij}	n	b^{ij}	c^{ij}	Ref.
Na+-Na+	5.0	1.0	11.7	51.8	1.7	1.7	4	_	_	[30]
Na+-Cl-	67.5	1.726	47.4	187.3	1.7	1.7	4	1.76	1	[30]
ClCl-	275.1	1.797	140	280	1.7	1.7	4	-	-	[30]
U ⁴⁺ -Na ⁺	1	5	0.001	0.001	1.9	1.9	4	10	0.001	[22]
U ⁴⁺ -Cl ⁻	304	1.85	95	925	1.9	1.9	4	1.258	1	This Work
$U^{4+}-U^{4+}$	1	5	100	1000	1.9	1.9	4	-	-	[31]
Th ⁴⁺ -Cl ⁻	210	1.75	95	925	1.9	1.9	4	1.258	1	This Work
Th^{4+} - Th^{4+}	1	5	100	1000	1.9	1.9	4	_	_	[31]
Th ⁴⁺ -Na ⁺	1	5	0.001	0.001	1.9	1.9	4	10	0.001	[22]

both the dipole-dipole and dipole-charge effects [24]. This is described in Eq. (7):

$$g_D^{ij}(r_{ij}) = 1 - C_D^{ij} e^{(-b_D^{ij}r_{ij})} \sum_{k=0}^4 \frac{(b_D^{ij}r_{ij})^k}{k!}$$
 (7)

The force field describing the interactions within the system, based on the Polarisable Ion Model (PIM) formalism, is, in principle, determined ab initio by reproducing the forces and dipoles obtained from DFT calculations on relatively small simulation cells, typically containing around one hundred atoms, following the consensus established by Salanne et al. [25,26]. However, as with all analytical force fields, PIM has inherent limitations in accurately capturing the equilibrium properties of materials, including their energetic, structural, and thermodynamic characteristics. In this work, we adopted a hybrid approach that integrates ab initio data with experimental constraints by incorporating the known experimental data. Among the interaction parameters, only those corresponding to the Th4+-Cl- and U4+-Cl- pairs required explicit determination, since the remaining parameters describing the other interactions were transferred directly from previously optimised halide systems (see Tables 1,2 for references). Starting from the initial ab initio-derived parameters [27,28], these values were further refined by applying the Lorentz-Berthelot mixing rules to adjust the dispersion term parameters, thereby improving agreement with experimental data while retaining consistency with the underlying ab initio reference data. This hybrid approach ensures that the final force field is both physically grounded and transferable across the studied systems.

The simulations were realised in the NPT and NVT ensembles using a Nosé-Hoover thermostat [29]. The NPT simulations, comprising 10^6 steps of 0.5 fs each, were conducted over a total time of 0.5 ns, during which the equilibrium volumes were extracted and molar enthalpies were determined. The NVT simulations used the same duration for each timestep but had a total runtime of 200 ps for equilibration, followed by 500 ps or 2 ns for the actual computations. The simulation temperature ranged from 873 to 1100 K. The compositions evaluated for the NaCl-ThCl₄ and NaCl-UCl₄ systems at various temperatures are documented in the Supplementary Information.

Table 2 Atomic polarisabilities for molten salt ions, all of the values are given in atomic units.

Ion	Polarisability	Ref.
Th ⁴⁺	7.696	Dewan et al. [23]
U^{4+}	5.8537	Dewan et al. [31]
Na ⁺	0.9	Ishii et al. [30]
Cl-	20	Ishii et al. [30]

2.2. Thermodynamic modelling

The thermodynamic modelling assessment was performed based on the CALPHAD (CALculation of Phase Diagram) method [32], using the FactSage software (version 8.2) [33]. Experimental data and results from MD simulations were used to optimise the excess parameters of the Gibbs energy functions for the phases present in this system.

2.2.1. Gibbs energies of pure compounds

The Gibbs energy of pure compounds is expressed as:

$$G(T) = \Delta_f H_m^0(298.15) - S_m^0(298.15)T + \int_{298.15}^T C_{p,m}(T)dT - T \int_{298.15}^T \frac{C_{p,m}}{T}dT$$
 (8)

where $\Delta_f H_m^0(298.15)$ is the standard enthalpy of formation and $S_m^0(298.15)$ the standard entropy at 298.15 K and standard pressure. $C_{p,m}$ is the heat capacity expressed as:

$$C_{p,m}(T) = a + bT + cT^2 + dT^{-2}$$
(9)

Selected thermodynamic functions for the end-members NaCl, ThCl₄ and UCl₄ are listed in Table 3. In this study, the thermodynamic functions for NaCl(cr,l) were sourced from the IVTAN database [34], except for the heat capacity of the liquid phase, which was recently updated by van Oudenaren et al. [20]. As for ThCl₄, the thermodynamic functions were adopted based on the guidelines provided by Rand et al. [35] and Capelli and Konings [36]. In line with the recent work by Dumaire et al. [7], the decision was made to neglect the low-temperature phase α -ThCl₄ in the thermodynamic modelling assessment since its existence and stability are still a source of controversy. The heat capacity of ThCl₄(I) (184.0 J·K⁻¹·mol⁻¹) was directly obtained from the output of the PIM-MD simulations. This differs from the value used in the recent work of Dumaire et al. [7] which follows the estimated values by Capelli and Konings [36]. For UCl₄, the functions used are from the critical review and reassessment conducted in 2023 by Yingling et al. [17] except for the heat capacity of UCl₄(1) (177.0 J·K⁻¹·mol⁻¹) which was again directly obtained from the output of the PIM-MD simulations. For the intermediate stable in the pseudobinary system NaCl-ThCl₄, i.e., Na₂ThCl₆, the Neumann-Kopp approximation [37] was used for the heat capacity. For the intermediate in the pseudobinary system NaCl-UCl₄, i.e., Na₂UCl₆, the heat capacity values are the same as in the assessment conducted in 2023 by Yingling et al., while the enthalpy of formation and standard entropy have been reoptimised [17].

2.2.2. Liquid solution

The excess Gibbs energy terms of the liquid solution are represented in this work using the quasi-chemical formalism in the quadruplet approximation, as proposed by Pelton et al. [40]. This method has demonstrated its strengths for modelling molten chloride and fluoride salt systems [16,18]. Fig. 1 provides an example of a quadruplet, enabling the representation of short-range ordering. The excess Gibbs energy parameters optimised here are associated with the second-nearest neighbor

Table 3
Thermodynamic functions used in the CALPHAD model in this work. The heat capacity is expressed as the following polynomial: $C_{p,m}(T) = a + bT + cT^2 + dT^{-2}$. Optimised values in this work from MD data and values determined as part of the CALPHAD assessment are marked in bold. Liquid thorium and uranium chloride are modelled as a $[An_2^{[XI]}Cl_8(I)-An^{[VI]}Cl_4(I)]$ mixture with $g_{An^{[VI]}}^0Cl_4(I) = \frac{1}{2}g_{An^{[XI]}Cl_8}^0(I) + 150,000 \text{ J} \cdot \text{mol}^{-1}$.

Compound	$\Delta_f H_m^o(298)$	S _m (298)	$C_{p,m}(T)$ (J·K ⁻¹	$C_{p,m}(T) (J \cdot K^{-1} \cdot mol^{-1}) = a + bT + cT^{2} + dT^{-2}$			Temperature	Source
	(J·mol ⁻¹)	$(J{\cdot}K^{-1}{\cdot}mol^{\cdot 1})$	a	b	с	d	range (K)	
NaCl(cr)	-411.260	72.15	47.72158	0.0057	1.21466 · 10-5	-882.996	298.15–1074	[20]
NaCl(l)	-390.853	83.30	68	_	_	_	298.15-2500	[20]
NaCl(g)	-181.420	229.794	37.364	0.00071	_	-163,206.1	298.15-3000	[38]
$Na_2Cl_2(g)$	-566.100	325.432	83.13295	$3.8671 \cdot 10^{-6}$	_	-402,023.30251	298.15-6000	[39]
$ThCl_4(cr)$	-1186.300	183.499	120.293	0.0232672	_	-615,050	298.15-6000	[7]
$ThCl_4(l)$	-1162.064	176.93	184	-	_	-	298.15-2500	[7][this work]
$Th_2Cl_8(l)$	-2,324,128	353.868	368	_	_	_	298.15-2500	[this work]
$ThCl_4(g)$	-950.000	403.40	107.721	$2.993 \cdot 10^{-4}$	$-6.023 \cdot 10^{-8}$	-573,880	298.15-6000	[36][this work]
$Na_2ThCl_6(cr)$	-2046.000	329.0	215.73616	0.0346672	$2.42932 \cdot 10^{-5}$	-616,815.992	298.15-703	[7][this work]
$UCl_4(cr)$	-1018.800	197.2	116.362	0.03108	_	-340,400	298.15-6000	[36]
$UCl_4(l)$	-998.606	200.77	177	-	_	-	298.15-2500	[36][this work]
$U_2Cl_8(l)$	-1997.2127	401.53	354	_	_	_	298.15-2500	[this work]
$UCl_4(g)$	-815.400	410.90	110.634	$3.2375 \cdot 10^{-3}$	$-3.12 \cdot 10^{-7}$	-715,600	298.15-6000	[36][this work]
$Na_2UCl_6(cr)$	-1877.0	343	208.2	0.06372	-	-34,040	298.15-2500	[17][this work]



Fig. 1. Illustration of the hypothesised quadruplet unit in molten salt, highlighting the first-nearest neighbours (FNN) and second-nearest neighbours (SNN). FNN are of opposite charges, while SNN possess equal charges.

(SNN) exchange reaction:

$$(A - X - A) + (B - X - X) \rightarrow 2(A - X - B)\Delta g_{AB/X}$$
 (10)

where A and B denote the cations and X represents the anions.

Moreover, to account for the formation of molecular species and formation of network structures in the salts investigated herein, we introduce monomeric as well as dimeric species on the cationic sublattice, as done in our previous works [19–22]. We refer the reader to the latter articles for a detailed description of the mathematical formalism adopted.

As shown in section 3 in this work, at low concentrations of $AnCl_4$, most An^{4+} ions exist as monomers with predominantly 6-fold coordination, forming $[AnCl_6]^{2-}$ complexes. At higher concentrations of $ThCl_4$ and UCl_4 , the formation of dimers, trimers, and eventually polymers is observed. One dimer for each system was selected $(Th_2Cl_{11}^{3-}$ and $U_2Cl_{11}^{3-})$, which represents all species of higher nuclearity in the model, following the recommendations in [41]. The selection of these specific complex ions was based on the PIM-MD results in Section 3. For NaCl-ThCl $_4$ system, this is moreover in line with research conducted by Photiadis et al. [42]. The cation–cation coordination numbers in this study were determined based on the stoichiometry of the coordinated complexes and dimers, as done in our previous works.

The cation–cation coordination numbers selected for the models are listed in Table 4.

The optimised excess Gibbs energy parameters for the $(Na,An)Cl_x$ liquid solution (An = Th, U) are presented in Eqs. (11)-(14).

$$\Delta NaTh[VI]/Cl_2 = -77000 - 5000\chi_{NaTh[VI]/Cl_2}$$
(11)

$$\Delta NaTh_2[XI]/Cl_2 = -38000 - 10 \cdot T + 33000 \chi_{NaTh_2[XI]/Cl_2}$$

$$-16000 \chi_{Th_2[XI]Na/Cl_2}$$
 (12)

 Table 4

 Cation-cation coordination numbers of the liquid solution.

A	В	Z^A_{AB/Cl_2}	Z^B_{AB/Cl_2}	Z^{Cl}_{AB/Cl_2}
Na^+	Na^+	6	6	6
$An_{[VI]}^{4+}$	$An_{[VI]}^{4+}$	6	6	1.5
$An_{2[XI]}^{6+}$	$An_{2[XI]}^{6+}$	6	6	0.75
$An_{[VI]}^{2[II]}$	$An_{2[XI]}^{6+} \ An_{2[XI]}^{6+}$	6	6	1
Na^+	$An_{[VI]}^{4+}$	3	6	2
Na^{+} $An^{4+}_{[VI]}$ $An^{6+}_{2[XI]}$ $An^{4+}_{[VI]}$ Na^{+}	$An_{2[XI]}^{8+}$	2	6	1.09

3. Results & discussion

3.1. Study of UCl₄ and ThCl₄ melts by molecular dynamics simulations

3.1.1. Density and molar volume

The simulated densities and molar volumes of ThCl $_4$ and UCl $_4$ using our optimised force field parameters are depicted in Figs. 2 and 3 in the temperature range 870–1100 K, and are compared to the previously reported experimental data.

The density of liquid UCl_4 was investigated in the literature using hydrostatic weighing by Bogacz et al. [13], a quartz pycnometer by Kuroda et al. [12], and the maximum bubble pressure method by Desyatnik et al. [15]. The three independent experimental studies on UCl_4 density are in rather good agreement with each other, and our calculated density reproduces well the measured values.

In Fig. 2, it is evident that the simulated density of ThCl₄ markedly diverges from experimental values, recent AI-MD computational results by Wang et al. [43] and recent PIM-MD simulations by Pireddu et al. [28]. However, an inconsistency was noticed in the literature: the experimental density of liquid ThCl₄, as reported by Kuroda et al. [12], surpasses that of the published data on UCl₄ (the reported molar volume of liquid ThCl₄ is lower than that of UCl₄, respectively). Such a discrepancy is puzzling, given that ThCl₄ and UCl₄ are isostructural compounds in the solid state, and expected to have a similar local structure in the liquid state. Following the decrease in ionic radius along the actinide series, one would expect the density of UCl₄ to be higher than that of ThCl₄ (thus the molar volume of UCl₄ to be lower than that of ThCl₄).

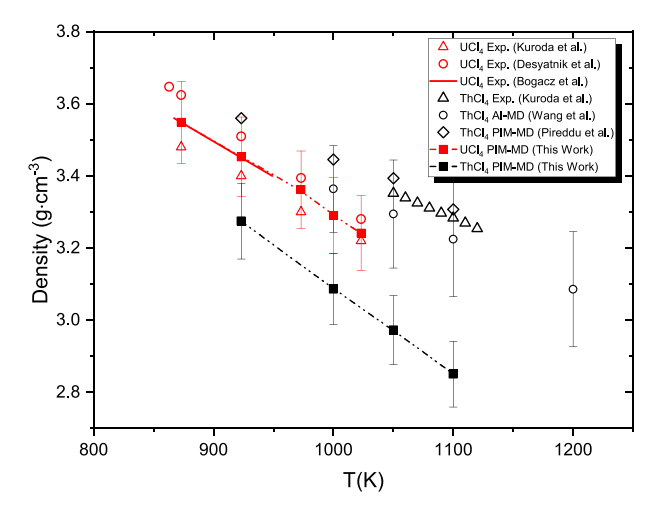


Fig. 2. Simulated density of liquid UCl_4 and $ThCl_4$ compared to experimental values determined by Desyatnik et al. [15] and Kuroda et al. [12,14], a linear fit to experimental data from Bogacz et al. [13], PIM-MD data from Pireddu et al. [28] and AI-MD data from Wang et al. [43].

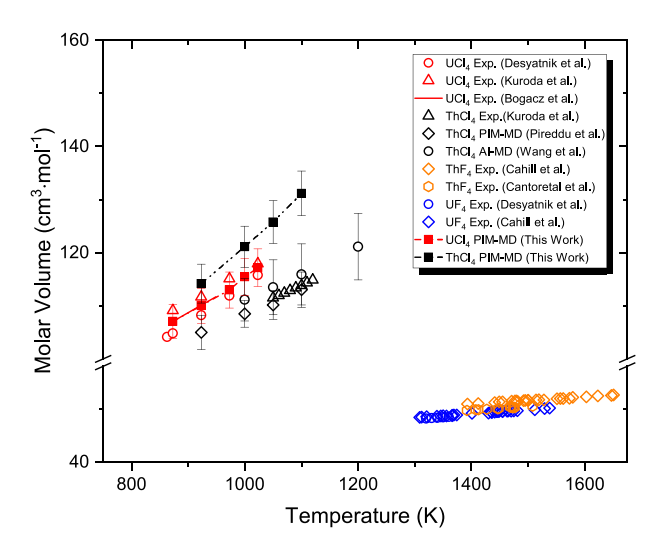


Fig. 3. Simulated molar volume of liquid UCl_4 and ThCl_4 compared to experimental values determined by Desyatnik et al. [15] and Kuroda et al. [12,14], a linear fit to experimental data from Bogacz et al. [13], PIM-MD data from Pireddu et al. [28] and AI-MD data from Wang et al. [43]. The errors in the data from this study correspond to the two standard deviations of the calculated MD values.

A comparable trend has been confirmed for the lanthanide chlorides by Goloviznina et al. [44], who reported a systematic increase in density along the lanthanide series in their PIM-MD simulations. In the equivalent fluoride salts, the densities and molar volumes respect this trend: UF₄ has a higher density than ThF₄ as reported by Kirshenbaum et al. [45]. It is conjectured here that although the absolute density values reported by Kuroda et al. [12] might be inaccurate, and need confirmation, their relative variations with temperature remain reliable as they show a similar slope to the uranium data. In fact, the thermal expansion coefficient of liquid ThCl4, as reported by Kuroda et al. [12], closely matches the values reported for liquid UCl₄ by the three aforementioned sources. This is also the case for liquid actinide fluorides, where the thermal expansion coefficients of UF₄ and ThF₄ are highly comparable. An explanation for the higher-than-expected density values as reported by Kuroda et al. [12] could be the presence of impurities. These impurities would need to have a higher density than pure ThCl₄ and be relatively

Table 5Comparison of heat capacity calculated in this work with literature data.

Compound	$Cp~(J{\cdot}K^{-1}{\cdot}mol^{-1})$	Method	Source
ThCl ₄	184 ± 8 167.4 ± 10 188 ± 5 168.3 ± 17	PIM-MD Estimated PIM-MD AI-MD	This Work Rand et al. [46] Pireddu et al. [28] Wang et al. [43]
UCl ₄	177 ± 8 168 163 ± 5	PIM-MD Review Experimental	This Work Capelli and Konings [36] Popov et al. [48]

inert. Potential candidates include ThO_2 , $ThOCl_2$ and thorium metal. Additionally, the high volatility of pure $ThCl_4$ and UCl_4 poses experimental challenges in obtaining accurate density measurements, which might explain the observed discrepancy.

3.1.2. Heat capacity

The heat capacities of the pure compounds $AnCl_4$ were calculated from the simulations using linear fits on the internal energy-temperature graphs. Although the heat capacity of liquid $ThCl_4$ has not yet been experimentally determined, AI-MD data from Wang et al. and estimations from Rand et al. [46] are available, as listed in Table 5. The heat capacity calculated from our PIM-MD simulations aligns well with the selected literature data within the reported uncertainties. This is encouraging, as AI-MD methods have also proven to match experimental data for other actinide halides [47].

For UCl4 we calculate that the heat capacity is remarkably similar to that of liquid ThCl₄. These results fall within each other's error margins, indicating no statistically significant difference between the two. Both values are higher than the earlier reported experimental value by Popov et al. [48], based on a direct heating method with a continuously measured heat input in a quartz calorimeter vessel coated on the outside with silver foil. However, given that the experimental data are derived from a single source and considering the challenges associated with measuring the heat capacity of liquid UCl4 due to its high volatility, this discrepancy is considered to be within an acceptable margin. It is also important to note that partial vaporisation of the melt during measurement could result in a lower observed heat capacity. This near-equivalence in heat capacity of liquid ThCl₄ and UCl₄ is consistent with trends observed for analogous systems: Tosolin et al. [49] have shown that UF4 and ThF4 exhibit nearly identical heat capacities, and similar behaviour has been reported by Goloviznina et al. [44] for lanthanide trichlorides, where PIM-MD simulations revealed minimal variation across the series. In addition, Pireddu et al. [28] reported comparable findings for actinide trichlorides using the same simulation method. These converging lines of evidence suggest that this thermodynamic similarity is a general feature of f-block halides, and supports the expectation that actinide tetrachlorides such as UCl4 and ThCl4 should likewise display closely matching heat capacities.

3.1.3. Local structure

The Radial Distribution Function (RDF) and average Coordination Number (CN) were calculated for the simulations at 1000 K. Fig. 4 illustrates the pairwise radial distribution functions (An-Cl, An-An, and Cl-Cl) in molten ThCl₄ and UCl₄. As anticipated, these RDFs exhibit many similarities to those of ThF₄ and UF₄ as determined by Ocádiz-Flores et al. [50]. The RDF analysis reveals that, despite the presence of long-range order in the molten state, there is a distinct structure of interlocking anionic and cationic coordination shells. Specifically, there are two An-Cl (An = Th, U) shells visible for each RDF, centred at 2.53 Å and 5.42 Å for Th-Cl, respectively, and 2.48 Å and 5.33 Å calculated at a 1000 K, for U-Cl respectively, before stabilising around the average value of g(r) = 1. Furthermore, similar to ThF₄ and UF₄, the first An-An shell exhibits a shoulder which is also observed by Wang et al. [43] using AIMD. Another notable similarity to fluorides is that ThCl₄

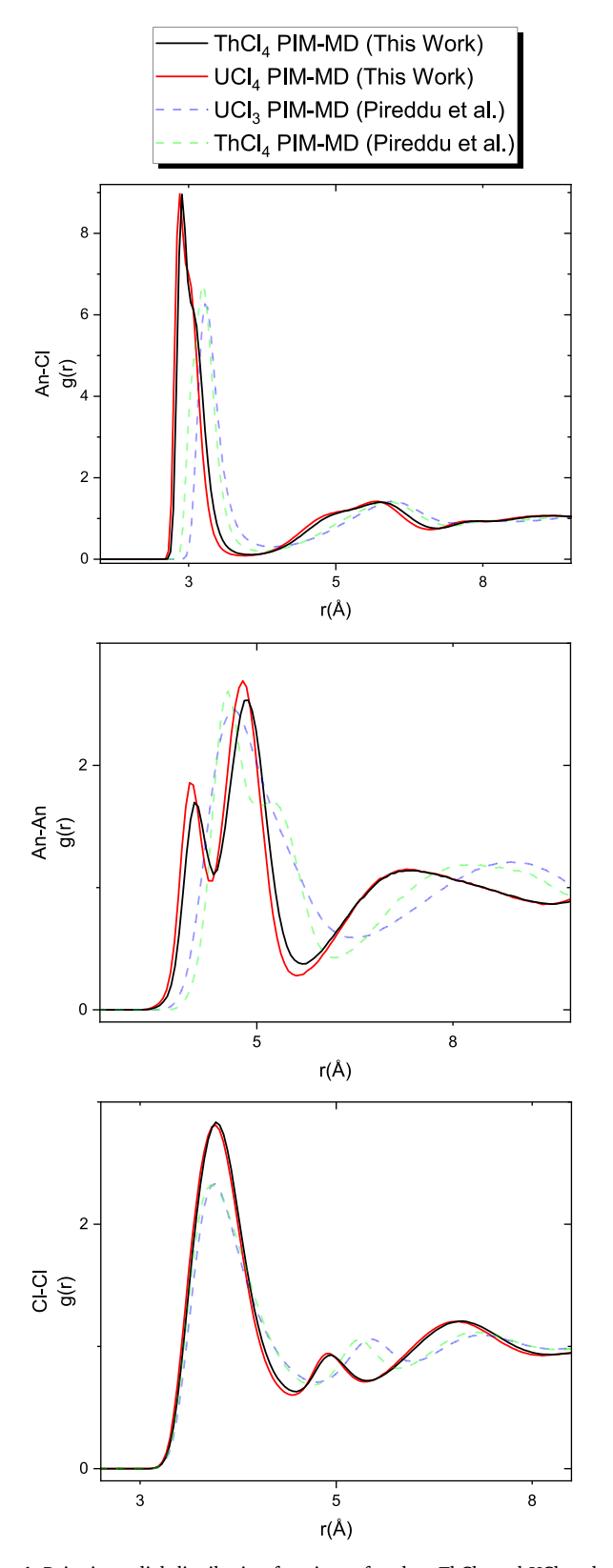


Fig. 4. Pairwise radial distribution functions of molten $ThCl_4$ and UCl_4 calculated with PIM-MD at T=1000 K.

and UCl4 are isostructural not only in their crystalline forms, but also in the melt. The only distinction is a slight contraction in the An-Cl bond length (rAnCl). An analogous trend has been reported for ThF₄ and UF₄ by Ocádiz-Flores et al. [50], and for the lanthanide trichlorides

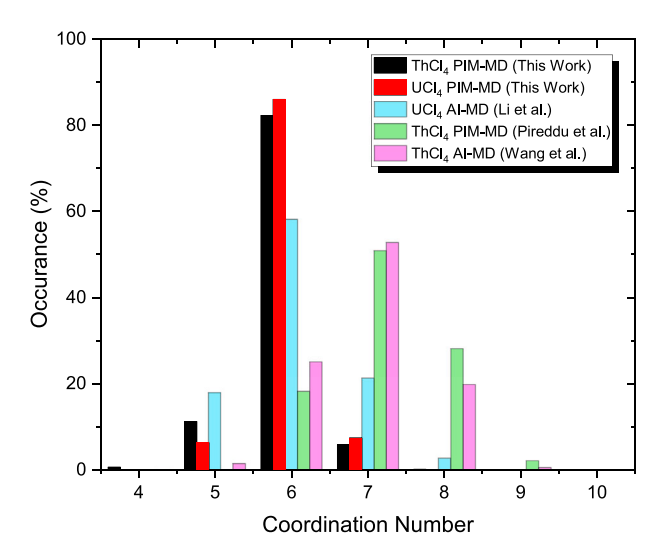


Fig. 5. Distribution of coordination numbers for ThCl₄ and UCl₄ from different studies. Results from the present PIM-MD simulations are shown for ThCl₄ (black) and UCl₄ (red) at T=1000~K. These are compared with AI-MD data for UCl₄ from Li et al. [51] (cyan), PIM-MD data for ThCl₄ from Pireddu et al. [28] (green), and AI-MD results for ThCl₄ from Wang et al. [43] (magenta). The predominance of six-fold coordination is evident across most data sets, with notable deviations in Wang et al.'s AI-MD results and Pireddu et al.'s PIM-MD results, where higher coordination numbers are favored.

by Goloviznina et al. [44], where the most probable $\rm Ln^{3+}$ -Cl⁻ distance decreases systematically from 2.78 Å for $\rm La^{3+}$ to 2.65 Å for $\rm Eu^{3+}$ as a direct consequence of the ionic radius contraction across the lanthanide series. Coincidentally, Goloviznina et al. [44] reported an average contraction of 0.025 Å per increase in atomic number, which matches well with the 0.05 Å reduction we observe between Th-Cl (2.53 Å) and U-Cl (2.48 Å). This systematic contraction is consistent with the actinide ionic radius trend and provides a structural basis for the differences in density observed between ThCl₄ and UCl₄.

The calculated average coordination of the Th⁴⁺ cation at 1000 K is 6.0. Here, the 6-fold coordinated complex [ThCl₆]²⁻ dominates with a fraction around 0.82, while the 5- and 7-fold coordinated [ThCl₅] and $[ThCl_7]^{3-}$ exist in equilibrium, representing fractions of 0.10 and 0.07, respectively. The remaining 0.01 fraction comprises minor amounts of 4-, 5-, 8-, and 9-coordinated species. This aligns well with the experimental data reported by Photiadis et al. [42], who observed a similar distribution using Raman spectroscopy. However, it contradicts the findings of Wang et al. [43], who calculated using AI-MD that the 7-fold coordinated complex is dominant in pure liquid ThCl₄ at 1100 K, with an average coordination of 6.90. The exact reason for this discrepancy is difficult to determine. One possible explanation is a link between the higher coordination number and increased density. While higher coordination might be expected to contribute to an increased density through more efficient packing, it is just one of several factors that must be considered in the local structure of the liquid, and the 3-dimensional network structure of oligomeric chains must also play a key role. Thus, the relationship between coordination number and density is certainly complex, and should vary depending on the specific properties of the melt.

For UCl₄ the calculated average coordination at 1000 K is 6.0, nearly identical to that of ThCl₄. It is observed that the 6-fold coordinated $[UCl_6]^{2-}$ dominates with a fraction of 0.86, alongside minor contributions from the 7-fold coordinated $[UCl_7]^{3-}$, which constitutes a fraction of 0.07, and the 5-fold coordinated $[UCl_5]^{1-}$ at 0.06. Additionally, the remaining fraction, approximately 0.01, comprises minor amounts of 4-, 8- and 9-coordinated species. Although there are no experimental data to compare to, it is possible to compare to an AIMD study performed

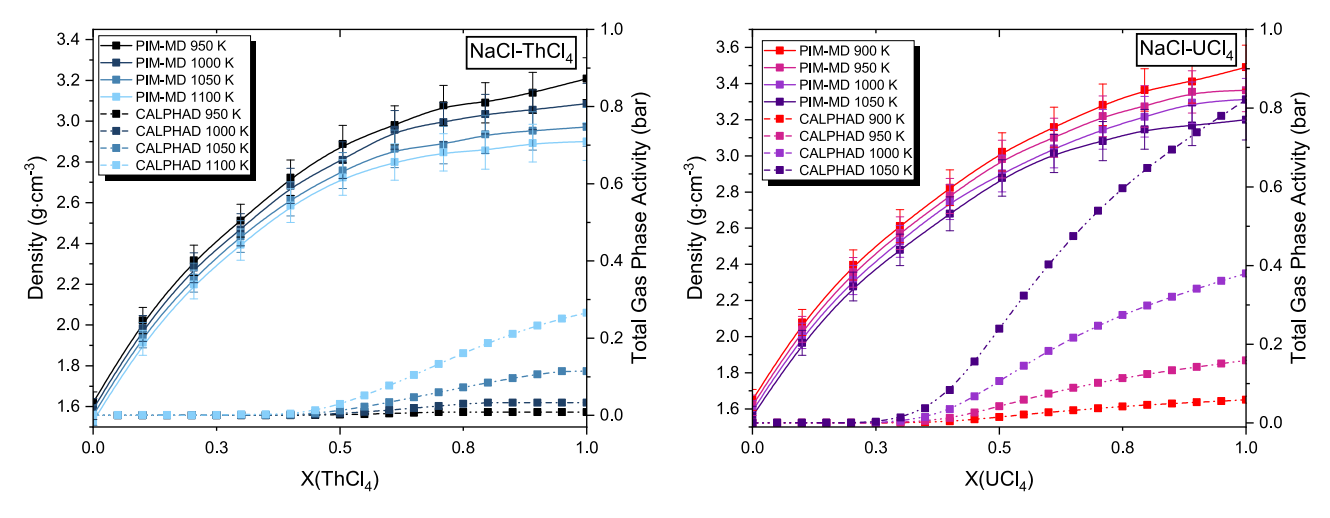


Fig. 6. Density evolution and total activity of gaseous species of the $(Na,An)Cl_x$ (An = Th, U) melts as a function of composition: (left) NaCl-ThCl₄ and (right) NaCl-Ucl₄. The calculated activity is based on the optimised vapourpressure of AnCl₄ and the CALPHAD models for NaCl-AnCl₄. Data are shown for NaCl-ThCl₄ at T = 950, 1000, 1050 and 1100 K and for NaCl-Ucl₄ at T = 900, 950, 1000 and 1050 K.

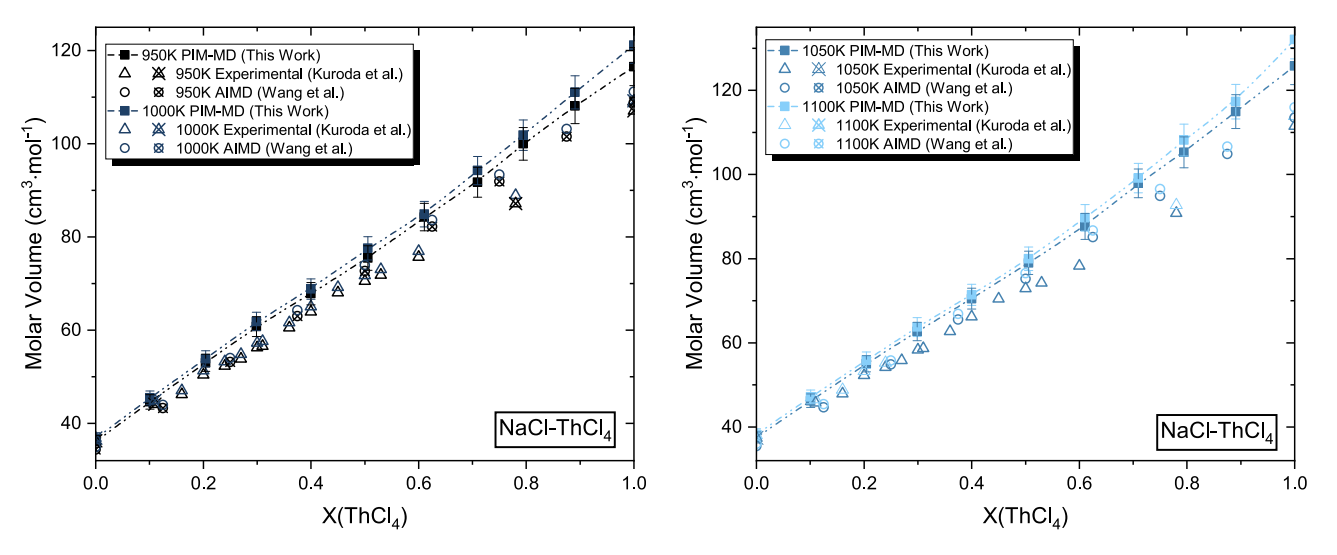


Fig. 7. Molar volume evolution of the $(Na,Th)Cl_x$ melt at temperatures T=950, 1000 K (Left) and T=1050, 1100 K (Right), analysed as a function of the molar fraction of $ThCl_4$. The calculated data are compared to experimental data from Kuroda et al. [12] and AIMD data from Wang et al. [43].

by Bo Li et al. [51]. The results of that work show that the average coordination of UCl_4 at 1200 K is 6.03, in very good agreement with the present study.

We see that $ThCl_4$ and UCl_4 exhibit remarkably similar coordination numbers, both centred around six-fold coordination. This trend is consistent with observations in other f-block halide systems. For instance, a comparable coordination behaviour was reported in lanthanide trichlorides by Goloviznina et al. [44], and in actinide trichlorides by Pireddu et al. [28]. Fig. 5

3.2. Study of NaCl-AnCl $_4$ melts by molecular dynamics

3.2.1. Density and molar volume

To enhance comparability with the simulations performed on the binary systems NaCl-UCl₄ and NaCl-ThCl₄, the limited number of experimental data points from the literature [12,15,52] were extended beyond their original temperature range. In the following figures, data from the literature extrapolated outside of the measured temperature range are indicated by a symbol with a cross (i.e., \boxtimes), whereas regular data points within the measured temperature range are represented without a cross (i.e., \square).

The densities and molar volumes of the binary mixtures were calculated based on the average dimensions of NpT ensemble simulation cells across different temperatures and compositions, as illustrated in Fig. 6. The data show that as temperature increases, the density decreases, resulting in an increase in molar volume due to thermal expansion. Notably, beyond 1150 K for NaCl-ThCl₄ and 1050 K for NaCl-UCl₄, respectively, the density starts to decline at higher concentrations of AnCl₄, which we attribute to the partial vaporisation of the melt. This is further supported by the CALPHAD calculated activities of AnCl₄(g) at various temperatures and compositions. Fig. 6 highlights that significant vaporisation of the melt occurs at elevated temperatures. This is not unexpected given the low boiling points for ThCl₄ [53] and UCl₄ [54] at 1205 K and 1064 K, respectively. Therefore, when discussing the results, appropriate temperature ranges are used, where the vapour pressure above the melt remains low.

Fig. 7 compares the calculated MD molar volume in the $(Na,Th)Cl_x$ melt to data from literature. As previously discussed, it is suggested here that although the absolute density values reported by Kuroda et al. [12] may be questionable, their relative variations with temperature remain reliable. This is reflected in Fig. 7, where the simulated molar volumes

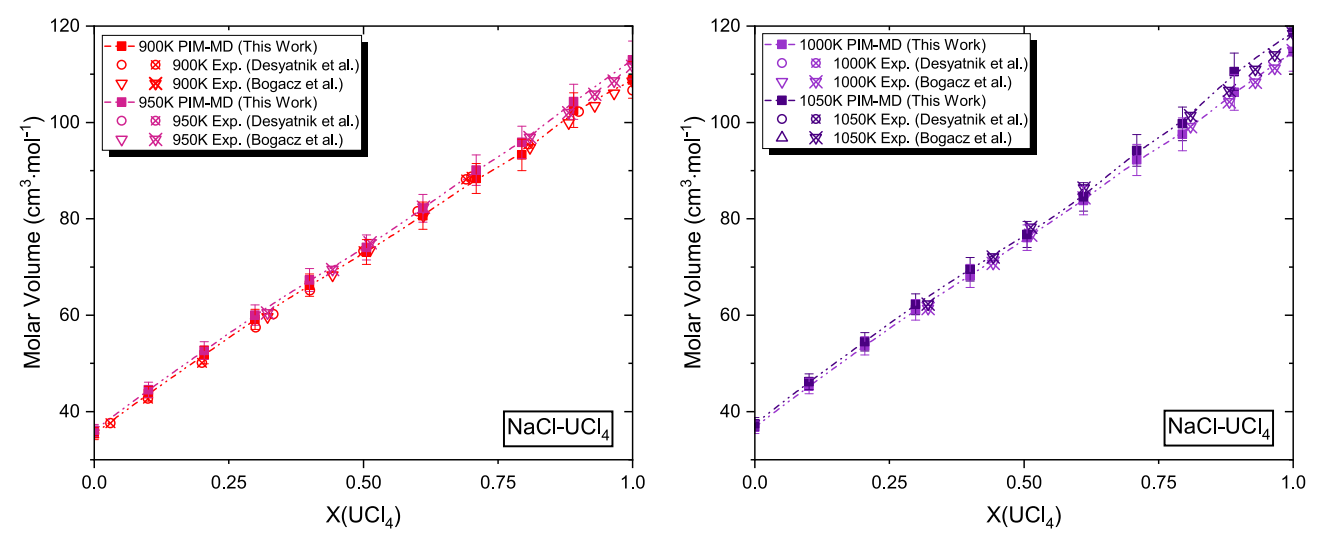


Fig. 8. Molar volume evolution of the $(Na,U)Cl_x$ melt at temperatures T = 900, 950 K (Left) and T = 1000, 1050 K (Right), analysed as a function of the molar fraction of UCl_4 . The calculated data are compared to experimental data from Desyatnik et al. [52] and Bogacz et al. [13].

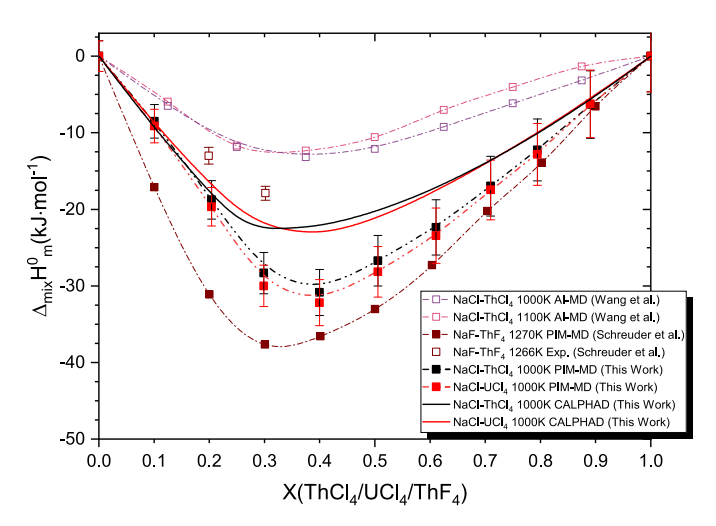


Fig. 9. Mixing enthalpies of the (Na,An)Cl_x (An = Th,U) melt as calculated by MD at T = 1000 K, compared to the AIMD data by Wang et al. [43] at T = 1100 K in the NaCl-ThCl₄ system. Furthermore, experimental and MD results at 1266 and 1270 K respectively on the NaF-ThF₄ by Schreuder et al. are included.

diverge more noticeably at higher fractions of ThCl₄, and consistently register higher molar volumes than the experimental data. However, the overall trend is well-represented across all temperatures.

Fig. 8 compares the calculated MD molar volumes in the $(Na,U)Cl_x$ melt to experimental data from Desyatnik et al. [52] and Bogacz et al. [13]. It can be observed that the calculated MD molar volumes are in excellent agreement with the experimental data across the observed temperature ranges.

3.2.2. Heat capacity and enthalpy of mixing

The mixing enthalpies for NaCl-ThCl₄ and NaCl-UCl₄, calculated from the MD simulations, are shown in Fig. 9. As anticipated from analogous fluoride systems [22], both NaCl-ThCl₄ and NaCl-UCl₄ exhibit negative values for the enthalpies of mixing. It is also observed that NaCl-UCl₄ exhibits a more negative enthalpy of mixing compared to NaCl-ThCl₄. Interestingly, the compositions of the minima in both curves coincide with the onset of polymerisation, a topic discussed in more detail later when the local structure is analysed.

Although no experimental data are available for direct comparison with these systems, previous work by Andersson et al. [47] on NaCl-UCl₃ has demonstrated that AI-MD simulations are highly effective in describing the mixing enthalpies of alkali actinide binary chloride mixtures. Consequently, the research by Wang et al. on NaCl-ThCl₄ serves as a valuable reference for comparison with our calculated mixing enthalpies [43]. Additionally, it is noteworthy that, similar to the trend seen in NaCl-UCl₃ and NaF-ThF₄, the magnitude of the enthalpy of mixing for both NaCl-UCl₄ and NaCl-ThCl₄ is significantly more negative than observed in experimental or AIMD data. The composition of maximum short-range ordering (SRO) for NaCl-UCl₄ and NaCl-ThCl₄ is calculated to be at X(AnCl₄) values of 0.39 and 0.37, respectively.

Fig. 10 presents the calculated heat capacities for the NaCl-ThCl₄ and NaCl-UCl₄ systems, plotted together across the entire composition range. As anticipated, the calculated heat capacity for pure NaCl aligns well with experimental data, as the potentials from Ishii et al. [30] were used. Although no direct experimental data exist for these specific mixed systems, the calculated NaCl-ThCl₄ data show good agreement with the AIMD results reported by Wang et al. [43].

Across the entire composition range, the NaCl-ThCl $_4$ system consistently exhibits a slightly higher heat capacity when compared to NaCl-UCl $_4$, however, when considering the error margins, this difference is negligible. When examining the excess heat capacity in Fig. 10, both melts demonstrate strong negative excess heat capacities of similar magnitude, with a distinct minimum around the composition of maximum SRO.

Other results obtained using the PIM method for similar systems, such as those by Schreuder et al. [22] for NaF-ThF $_4$ and Van Oudenaren et al. [20] for NaCl-UCl $_3$, show a similarly negative excess heat capacity, aligning closely with the results of the current study. This consistency across PIM studies strengthens the reliability of these findings.

3.2.3. Local structure and speciation

Fig. 11 displays the radial distribution functions, g(r), for selected ion–ion pairs in molten NaCl-ThCl₄ and NaCl-UCl₄ mixtures across a range of compositions. The RDFs are shown for An⁴⁺-Cl⁻, An⁴⁺-An⁴⁺, and Cl⁻-Cl⁻ correlations. A color gradient shows the mole fraction of AnCl₄, ranging from 0 (pure NaCl) to 1 (pure AnCl₄). These plots reveal the compositional evolution of both short- and intermediate-range structural order. Notably, the first peak in the An-Cl RDF, corresponding to the primary solvation shell, exhibits a clear decrease in intensity with increasing AnCl₄ content. This likely reflects increased competition

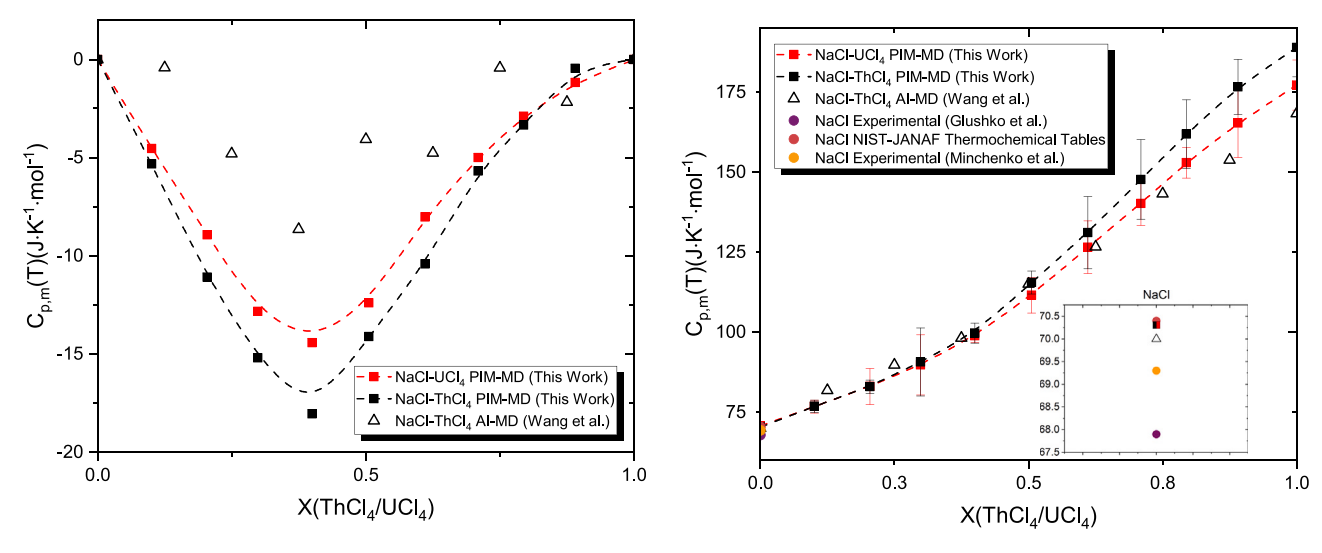
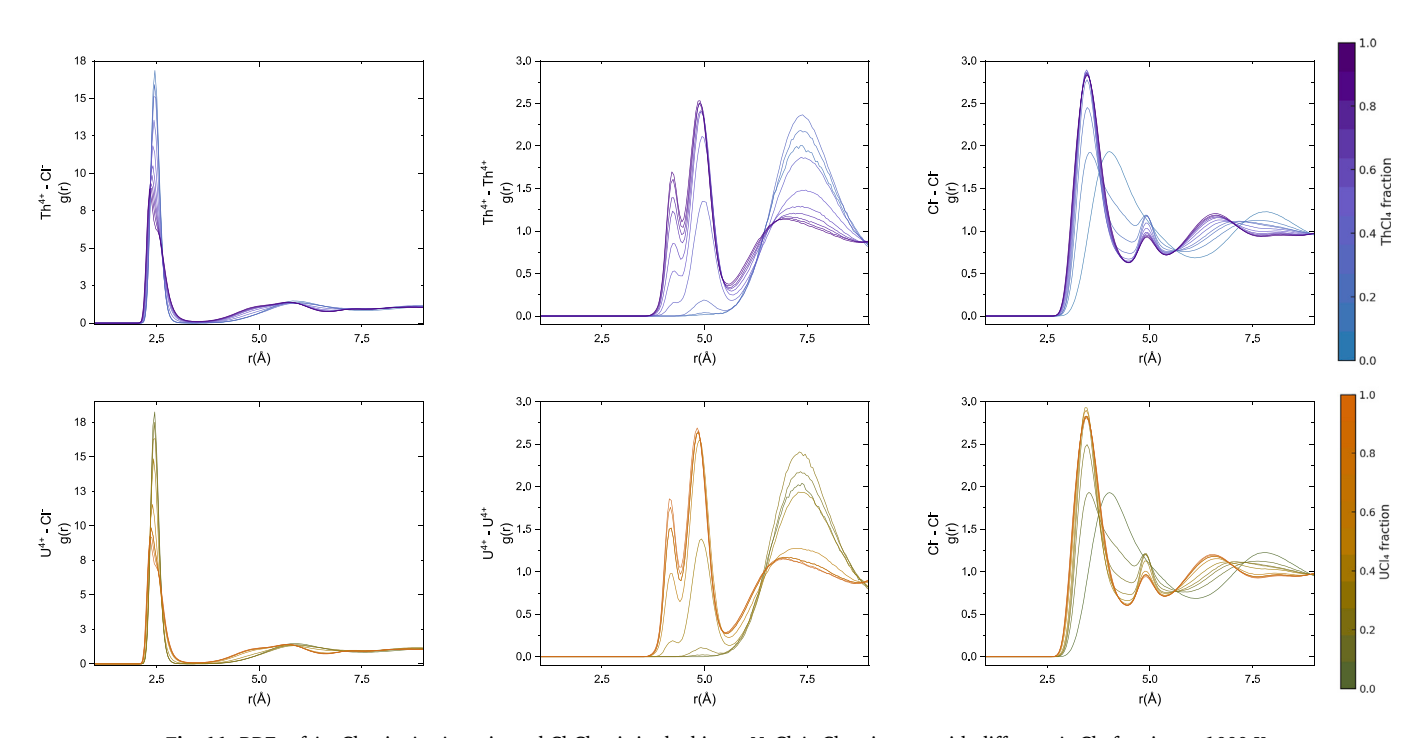


Fig. 10. Heat capacity (Left) or excess heat capacity (Right) of the $(Na,A)Cl_x$ (A = Th,U) melt, analysed as a function of the molar fraction of ACl₄. The errors in the data from this study correspond to two standard deviations of the calculated MD values.



 $\textbf{Fig. 11.} \ \ \textbf{RDFs of An-Cl pair, An-An pair, and Cl-Cl pair in the binary NaCl-AnCl}_{4} \ \ \textbf{mixtures with different AnCl}_{4} \ \ \textbf{fraction at 1000 K.}$

among An⁴⁺ cations for Cl⁻ anions, which weakens individual An⁴⁺-Cl⁻ interactions as the number of coordinating cations rises. Similar behaviour has been reported in other molten salt mixtures, including the AIMD studies of NaCl-ThCl₄ by Wang et al. [43], and the NaCl-UCl₄ and NaCl-UCl₃ systems examined by Li et al. [51].

Additionally, a distinct double feature in the An⁴⁺-Cl⁻ RDF, prominent at high AnCl₄ fractions, gradually diminishes and largely vanishes around $x(\text{AnCl}_4) = 0.3$ –0.4. This transition coincides with the disappearance of a corresponding double feature in the An⁴⁺-An⁴⁺ RDF, suggesting a shared structural origin. We attribute this behaviour to the onset of polymerisation within the melt: at higher AnCl₄ content, polynuclear complexes form that exhibit multiple characteristic An⁴⁺-Cl⁻ and An⁴⁺-An⁴⁺ distances, manifesting as split RDF features. As NaCl becomes the dominant component, these polymeric structures dissolve, leading to a

more uniform coordination environment and the collapse of the double features. $\,$

Fig. 12 depicts the distribution of complex anions at 1000 K for the NaCl-ThCl₄ and NaCl-UCl₄ systems, respectively. At low AnCl₄ concentrations, the melt is almost entirely comprised of six-coordinated complexes, forming stable $[{\rm AnCl_6}]^{2-}$ species. However, as the AnCl₄ fraction increases, five- and seven-coordinated complexes begin to emerge in nearly equal proportions in both systems. As a result, the average coordination number remains effectively constant near 6, as shown in the supplementary information. This behaviour aligns closely with the findings of Li et al. [51] for the NaCl–UCl₄ system, but deviates from the trend reported by Wang et al. [43] in their study of NaCl–ThCl₄, where a stronger deviation in coordination number was observed. The consistency between UCl₄ and ThCl₄ coordination trends in our simulations

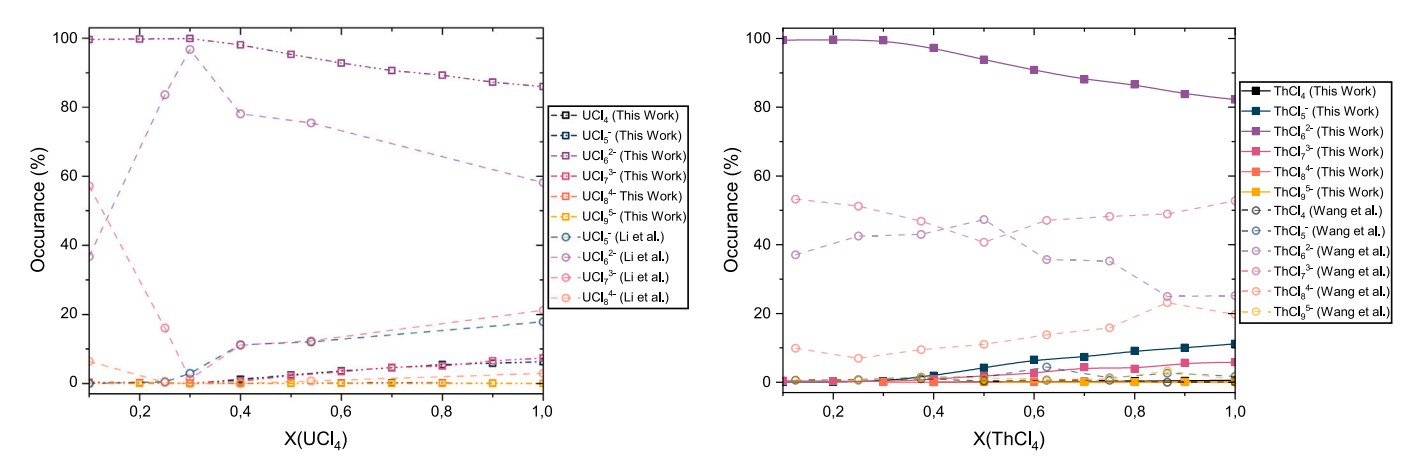


Fig. 12. Distribution of 4-,5-,6-,7-,8-,9-coordinated $[AnCl_n]^{m-}$ An = (Th,U) complexes calculated in this work versus composition in the NaCl-AnCl₄ system at 1000 K compared to AI-MD studies by Wang et al. [43]. and Li et al. [51].

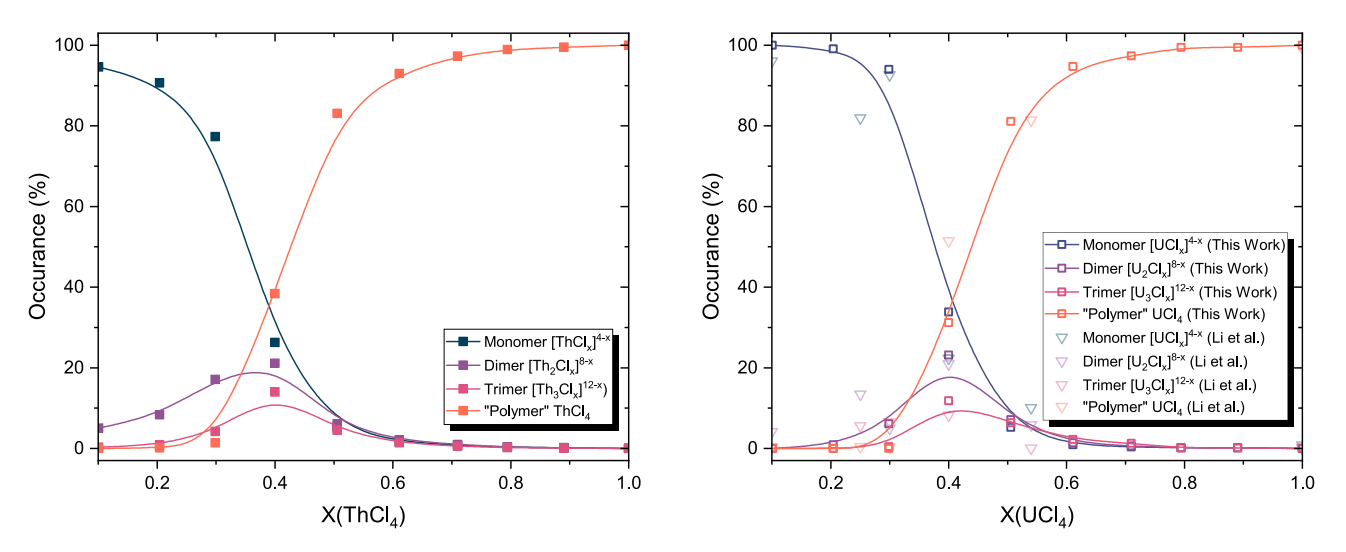


Fig. 13. Calculated chemical speciation at 1000 K of the NaCl-ThCl₄ system (Left) and NaCl-UCl₄ system (Right) calculated by MD compared to AI-MD data by Li et al. [51].

suggests that the coordination environments in ${\rm NaCl\text{-}AnCl_4}$ mixtures evolve in a structurally analogous manner.

Fig. 13 displays the calculated speciation at T=1000~K for both NaCl-AnCl₄ systems. This figure reveals that the UCl₄ and ThCl₄ based salts exhibit onset of polymerisation at a similar composition, likely due to the similar chemical bonding properties of U⁴⁺ and Th⁴⁺ valence shell electrons, as also reflected by the similar coordination numbers. For NaCl-UCl₄, the onset of polymerisation is in agreement with the AIMD results reported by Li et al. [51], reinforcing the validity of these findings. Finally, it is interesting to point out, that below $X(AnCl_4)=0.4$, in the composition range where monomers remain dominant along with dimers and trimers, the prevalent coordination of monomeric species in the thorium and uranium melt is (VI), as shown in Fig. 12, while (V) and (VII) coordinated monomers reach equivalent, but small fractions. This information was used to build the thermodynamic models as described hereafter.

3.3. Thermodynamic modelling

3.3.1. NaCl-ThCl₄

Using the coordination and speciation data derived from MD simulations at 1000 K, along with calorimetric data from the literature, including studies by Tanii et al. [55], Vokhmyakov et al. [56], and Oyamada [57], the CALPHAD model for the NaCl-ThCl $_4$ binary system,

as shown in Fig. 14, was developed. In this model, all monomers were represented by a single complex anion, the 6-coordinated $[ThCl_6]^{2-}$, which was selected due to its predominance across the entire composition range, as shown in Fig. 12. To represent the polymer chains, a single 11-coordinated dimer, $[Th_2Cl_{11}]^{3-}$, was selected, following the argumentation outlined in our recent review [41]. Notably, we did not include trimers in the model to avoid having to optimise too many degrees of freedom. Trimers are included in the modelling of the LiF-BeF₂ system [19], to reflect its much higher viscosity [41].

It can be seen in Fig. 14 that the model represents well the thermodynamic phase diagram events described in literature. The eutectic equilibria are calculated to be at compositions of $\{X(ThCl_4) = 0.26, T = 646 \text{ K}\}$ and $\{X(ThCl_4) = 0.46, T = 646 \text{ K}\}$, respectively, which is in good agreement with previous work by Ocádiz-Flores et al. [16].

The comparison between the mixing enthalpy from the CALPHAD model and the literature data shows that, while the overall trend is well captured, the magnitude of the mixing enthalpy is significantly larger in the CALPHAD model than in the AIMD results from Wang et al. [43] as can be seen in Fig. 9. However, the uncertainty associated with the AIMD results remains unknown. Fig. 15 demonstrates that the speciation and onset of polymerisation in the CALPHAD model are in excellent agreement with the MD simulation results calculated at 1000 K.

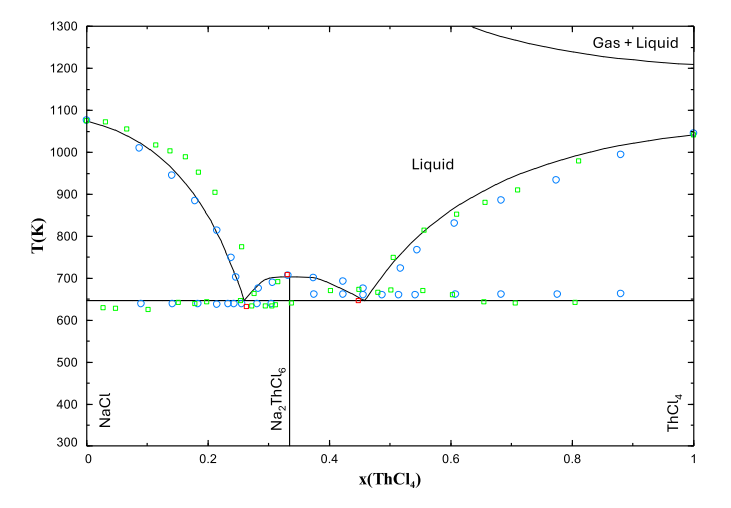


Fig. 14. NaCl-ThCl₄ phase diagram, as calculated in this work using the coupled structural thermodynamic model compared to available experimental data. The phase equilibria data were obtained by Tanii et al. $[\Box]$, Vokhmyakov et al. $[\Box]$ and Oyamada $[\circ]$.

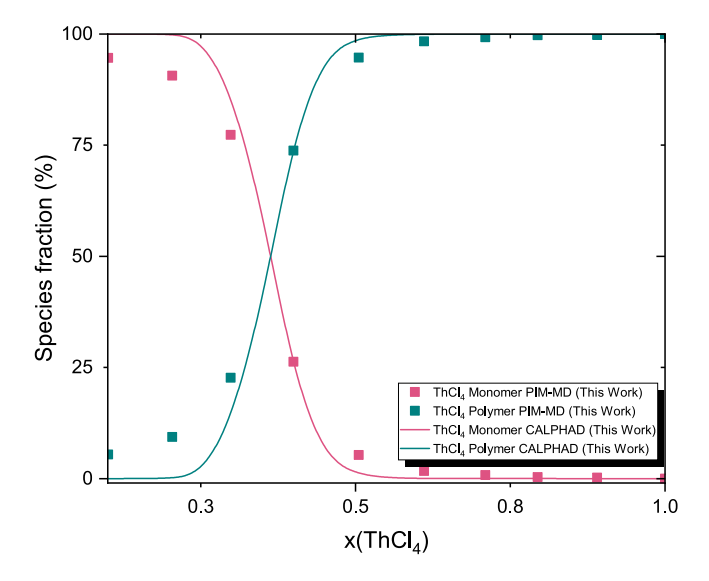


Fig. 15. Chemical speciation at 1000 K of the NaCl-ThCl₄ system as calculated by MD and with the CALPHAD model. Here all the monomers present in the MD calculations correspond to the 6-coordinated monomers $[ThCl_6]^{2-}$, and all the polymers present in the MD calculations correspond to the 11-coordinated dimers $[Th_2Cl_{11}]^{3-}$.

3.3.2. NaCl-UCl₄

The CALPHAD model for the NaCl-UCl $_4$ binary system, shown in Fig. 16, was developed using coordination and speciation data derived from MD simulations at 1000 K, in combination with calorimetric phase diagram data reported in the literature, including studies by Bogacz et al. [58], Kuroda et al. [59], and Thoma [60], as well as melting data for Na $_2$ UCl $_6$.

Given the close similarity in ionic radii between U^{4+} and Th^{4+} , and the comparable bonding environments observed in the MD simulations, the modelling approach for NaCl-UCl₄ was aligned with that of NaCl-ThCl₄. As such, all monomers were represented by a single 6-coordinated complex anion, $[UCl_6]^{2-}$, which is dominant up to approximately 30 mol% UCl_4 , beyond which polymeric species take over. A single 11-coordinated dimer, $[U_2Cl_{11}]^{3-}$, consistent with the structural model developed for Th^{4+} , was used to represent the polymeric fraction as it was among the most prevalent polymeric species observed

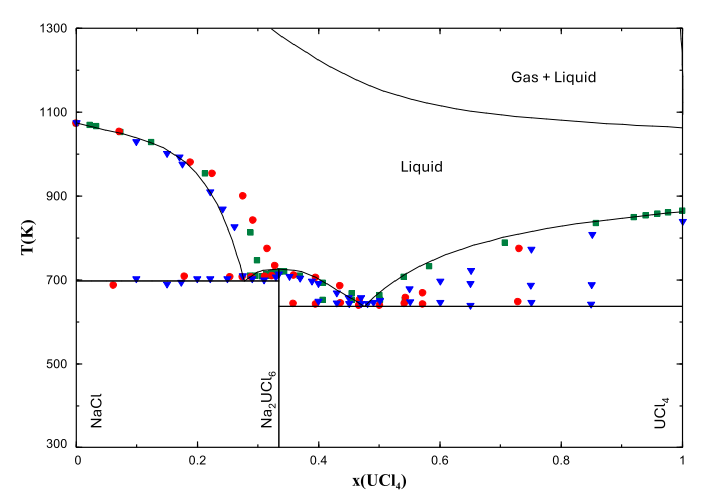


Fig. 16. The NaCl-UCl $_4$ phase diagram, as calculated in this work using the coupled structural thermodynamic model compared to available experimental data. The thermodynamic events were obtained by Bogacz et al. [\blacksquare], Kuroda et al. [\bullet] and Thoma [\blacktriangledown].

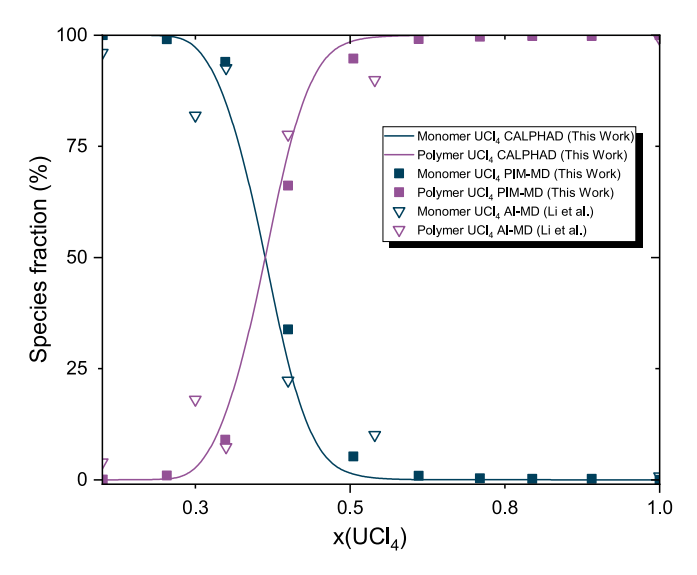


Fig. 17. Chemical speciation at 1000 K of the NaCl-UCl₄ system as calculated by MD and with the CALPHAD model. Here all the monomers present in the MD calculations correspond to the 6-coordinated monomers $[UCl_6]^{2-}$, and all the polymers present in the MD calculations correspond to the 11-coordinated dimers $[U_2Cl_{11}]^{3-}$. compared to AI-MD data by Li et al. [51].

in PIM-MD. As shown in Fig. 16, the model predicts two eutectic equilibria, at compositions of $X(UCl_4) = 0.28$ and $X(UCl_4) = 0.48$, with corresponding temperatures of 696 K and 636 K, respectively. Recent experimental studies performed in our group on the Na_2UCl_6 compound suggest it melts congruently [61]. Consequently, the thermodynamic functions of Na_2UCl_6 were reassessed accordingly (see Table 3), based on formation enthalpies reported by Martynova et al. [62] and adjusted within experimental uncertainty to ensure internal consistency.

Fig. 9 compares the mixing enthalpy predicted by the CALPHAD model with AIMD results from Wang et al. [43]. As with NaCl-ThCl₄, the overall trend is reproduced, but the magnitude of the mixing enthalpy remains significantly larger in the CALPHAD model. The speciation and onset of polymerisation predicted by the CALPHAD model align well with the MD simulations at 1000 K (Fig. 17).

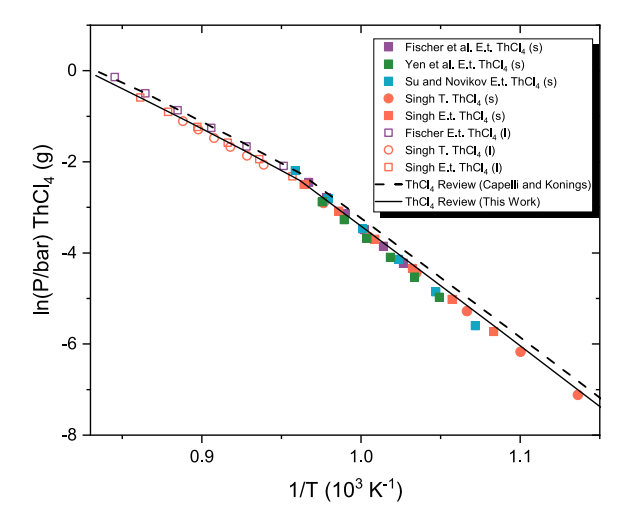


Fig. 18. Vapour pressure of ThCl₄ as a function of inverse temperature. Data are shown from evaporation temperature measurements [63–65] and transpiration [53], alongside the reoptimised model developed in this work.

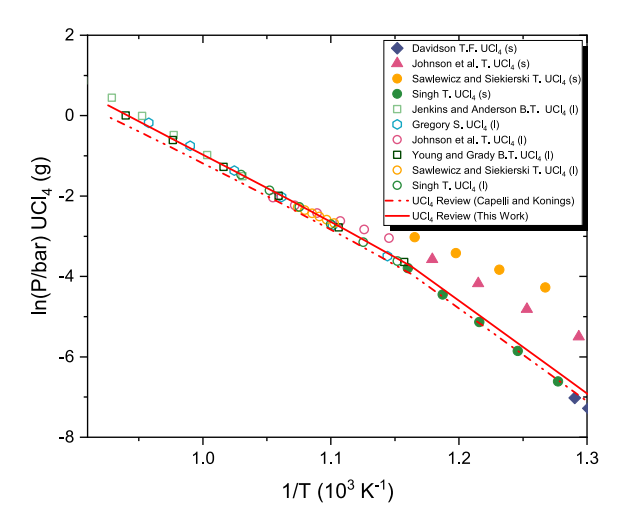


Fig. 19. Vapour pressure of UCl_4 as a function of inverse temperature. Experimental data from tube flow [66], transpiration [54,67,68], and boiling/static pressure methods [66] are shown together with the present reoptimised model.

3.3.3. Reoptimisation of thermodynamic functions for gaseous $ThCl_4(g)$ and $Ucl_4(g)$

As mentioned already, $ThCl_4$ and UCl_4 show rather high vapour pressure. Some inconsistencies among literature vapour pressure datasets were noticed, and a critical re-evaluation of the gas-phase thermodynamic functions of $ThCl_4$ and UCl_4 was therefore performed, to improve the reliability of the CALPHAD models. Starting from the evaluations of Capelli and Konings [36], we reoptimised those functions by fitting to selected vapour pressure data for $ThCl_4$ obtained by the evaporation temperature method [63–65] and transpiration method [53], and for UCl_4 from tube flow [66], transpiration [54,67,68], and boiling/static pressure measurements [66]. The resulting expressions reproduce the vapour pressure behaviour across the solid and liquid regimes with improved fidelity, as shown in Figs. 18 and 19.

3.3.4. Vapour pressures across the binary salt mixtures

While vapour pressure data have not been, to the best of our knowledge, reported in the literature above (NaCl-UCl₄) melts, Smirnov et al.

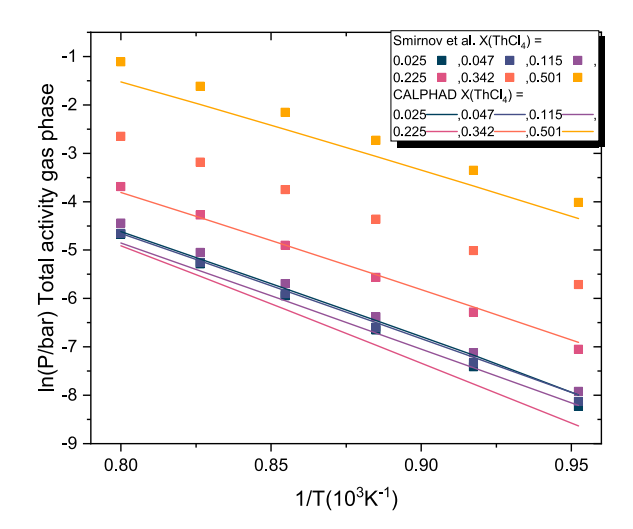


Fig. 20. Total gas-phase activity (ln(bar)) for the NaCl-ThCl₄ system at various mole fractions of ThCl₄. Experimental data from Smirnov et al. [69] are compared to CALPHAD model predictions (This Work) across six compositions.

[69] reported data for (NaCl-ThCl₄) salt mixtures. Fig. 20 shows the calculated vapour pressure over the NaCl-ThCl₄ melt at 973 K compared to the measurements reported by Smirnov [69]. The model underestimates the vapour pressure significantly in the range of 20–40 mol% ThCl₄. Interestingly, this is the region where Smirnov attributes the dominant gas-phase species to NaThCl₅(g), a gaseous species not currently included in the thermodynamic model. At higher ThCl₄ fractions (above 50 mol%), the agreement improves, suggesting the current model well captures the vaporisation behaviour when ThCl₄(g) becomes the primary species.

4. Conclusion

New force field parameters are reported in this work for the ThCl₄ and UCl4 molten salts, based on the Polarisable Ion Model. The structural, thermodynamic, and thermo-physical properties of the latter salts and their mixtures with NaCl were then scrutinised in the temperature range 900 to 1100 K. The output of the MD simulations was moreover used together with phase equilibria data in the literature to develop thermodynamic models of the NaCl-ThCl₄ and NaCl-UCl₄ systems that also reproduce the local structure and chemical speciation taking place within the melt. Our studies have highlighted the need to collect key thermophysical data that would help to confirm and improve the quality of PIM simulations on those systems. In particular, we note that uncertainties in the reported densities of ThCl₄ and UCl₄ remain unresolved, and highly recommend their remeasurement using modern techniques. Experimental investigation of the local structure of molten AnCl₄ (An = Th, U), for example via in situ EXAFS or neutron diffraction, is essential to validate the An-Cl distances and coordination environments predicted by the here presented molecular dynamics simulations.

For the NaCl–AnCl $_4$ binary systems, calorimetric measurements of the mixing enthalpy, confirmation of the herein presented eutectic compositions, and investigation of gaseous species such as NaAnCl $_5$ would also be highly beneficial to refine thermodynamic models.

CRediT authorship contribution statement

N.T.H. ter Veer: Writing – review & editing, Writing – original draft, Visualization, Validation, Methodology, Investigation, Formal analysis, Data curation, Conceptualization. W.K. de Vries: Investigation. C.T.C. Heyning: Investigation. T.F. Abbink: Investigation. A.E. Gheribi: Supervision. R.J.M. Konings: Writing – review & editing, Supervision, Investigation. A.L. Smith: Writing – review & editing, Project administration, Investigation, Funding acquisition, Conceptualization.

Declaration of competing interest

The authors declare the following financial interests/personal relationships which may be considered potential competing interests:

Anna L. Smith reports financial support was provided by Horizon Europe. If there are other authors, they declare that they have no known competing financial interests or personal relationships that could have appeared to influence the work reported in this paper.

Acknowledgments

The authors acknowledge funding from the MIMOSA project, grant number 101061142 funded by the European Union. Views and opinions expressed are however those of the author(s) only and do not necessarily reflect those of the European Union. Neither the European Union nor the granting authority can be held responsible for them.

Appendix A. Supplementary data

Supplementary data for this article can be found online at doi:10. 1016/j.mollig.2025.128590.

Data availability

Data will be made available upon request.

References

- [1] B. Merritt, M. Seneca, B. Wright, N. Cahill, N. Petersen, A. Fleming, T. Munro, Thermal conductivity characterization of fluoride and chloride molten salts using a modified transient hot-wire needle probe, Int. J. Thermophys. 43 (2022) 149.
- [2] J. Serp, M. Allibert, O. Beneš, S. Delpech, O. Feynberg, V. Ghetta, D. Heuer, D. Holcomb, V. Ignatiev, J.L. Kloosterman, et al, The molten salt reactor (MSR) in generation IV: overview and perspectives, Prog. Nucl. Energy 77 (2014) 308–319.
- [3] R. Roper, M. Harkema, P. Sabharwall, C. Riddle, B. Chisholm, B. Day, P. Marotta, Molten salt for advanced energy applications: a review, Ann. Nucl. Energy 169 (2022) 108924.
- [4] D. Holcomb, G. Flanagan, B. Patton, J. Gehin, R. Howard, T. Harrison, Fast spectrum molten salt reactor options, Ornl/tm-2011/105 (2011).
- [5] A. Mourogov, P. Bokov, Potentialities of the fast spectrum molten salt reactor concept: rebus-3700, Energy Convers. Manag. 47 (2006) 2761–2771.
- [6] O. Beneš, R. Konings, Thermodynamic evaluation of the NaCl-MgCl₂-UCl₃-PuCl₃ system, J. Nucl. Mater. 375 (2008) 202–208.
- [7] T. Dumaire, J.A. Ocádiz-Flores, R.J. Konings, A.L. Smith, A promising fuel for fast neutron spectrum molten salt reactor: NaCl-ThCl₄-PuCl₃, Calphad 79 (2022) 102496.
- [8] M.B. Schaffer, Abundant thorium as an alternative nuclear fuel: important waste disposal and weapon proliferation advantages, Energy Policy 60 (2013) 4–12.
- [9] C. Degueldre, M.J. Joyce, Evidence and uncertainty for uranium and thorium abundance: a review, Prog. Nucl. Energy 124 (2020) 103299.
- [10] A.L. Smith, Structure-property relationships in actinide containing molten salts a review: understanding and modelling the Chemistry of nuclear fuel salts, J. Mol. Liq. 360 (2022) 119426.
- [11] S. Jiang, Y. Liu, L. Wang, Z. Chai, W.-Q. Shi, The coordination Chemistry of f-block elements in molten salts, Chem. Eur. J. 28 (2022) e202201145.
- [12] R. Oyamada, S. Yoshida, T. Kuroda, Molecular volume of ThCl₄-NaCl system, Electrochem. Ind. Phys. Chem. 37 (1969) 417–419.
- [13] A. Bogacz, B. Ziólek, Electrical conductivities and densities of molten salts in systems MCI-UCl₄ (M= Na, K, Rb, Cs), Rocz. Chem. 44 (1970) 665.
- [14] T. Kuroda, T. Suzuki, Electric conductance of molten UCl₄ and molten salt mixtures containing UCl₄, J. Electrochem. Soc. Jpn. 29 (1961) E215–E217.
- [15] V. Desyatnik, S. Katyshev, S. Raspopin, Physicochemical properties of melts comprising mixtures of uranium tetrachloride with the chlorides of alkali metals, Sov. At. Energy 42 (1977) 108–112.
- [16] J.A.O. Flores, B.A. Rooijakkers, R.J. Konings, A.L. Smith, Thermodynamic description of the ACl-ThCl₄ (A = Li, Na, K) systems, Thermo 1 (2021).
- [17] J.A. Yingling, M. Aziziha, J. Schorne-Pinto, J.P.S. Palma, J.C. Ard, R.E. Booth, C.M. Dixon, T.M. Besmann, Thermodynamic assessment of CrCl₂ with NaCl-KCl-MgCl₂-UCl₃-UCl₄ for molten chloride reactor corrosion modeling, ACS Appl. Energy Mater. 6 (2023) 5868–5882.
- [18] D. Alders, J. Vlieland, M. Thijs, R. Konings, A. Smith, Experimental investigation and thermodynamic assessment of the BaCl₂–CeCl₃ system, J. Mol. Liq. 396 (2024) 123997.
- [19] A. Smith, E. Capelli, R. Konings, A.E. Gheribi, A new approach for coupled modelling of the structural and thermo-physical properties of molten salts. Case of a polymeric liquid LiF-BeF₂, J. Mol. Liq. 299 (2020) 112165.
- [20] G. van Oudenaren, J. Ocadiz-Flores, A. Smith, Coupled structural-thermodynamic modelling of the molten salt system NaCl-UCl₃, J. Mol. Liq. 342 (2021) 117470.
- [21] J. Ocádiz-Flores, A.E. Gheribi, J. Vlieland, K. Dardenne, J. Rothe, R.J. Konings, A.L. Smith, New insights and coupled modelling of the structural and thermodynamic properties of the LiF-UF₄ system, J. Mol. Liq. 331 (2021) 115820.

- [22] M.B. Schreuder, J.A. Ocádiz-Flores, A.E. Gheribi, O. Beneš, J.-C. Griveau, E. Colineau, R.J. Konings, A.L. Smith, Experimental and computational exploration of the NaF-ThF₄ fuel system: structure and thermochemistry, J. Phys. Chem. B 125 (2021) 8558–8571
- [23] L.C. Dewan, C. Simon, P.A. Madden, L.W. Hobbs, M. Salanne, Molecular dynamics simulation of the thermodynamic and transport properties of the molten salt fast reactor fuel LiF-ThF₄, J. Nucl. Mater. 434 (2013) 322–327. Special Section on Spent Nuclear Fuel.
- [24] K.T. Tang, J.P. Toennies, An improved simple model for the van der Waals potential based on universal damping functions for the dispersion coefficients, J. Chem. Phys. 80 (1984) 3726–3741.
- [25] A.E. Gheribi, D. Corradini, L. Dewan, P. Chartrand, C. Simon, P.A. Madden, M. Salanne, Prediction of the thermophysical properties of molten salt fast reactor fuel from first-principles, Mol. Phys. 112 (2014) 1305–1312.
- [26] M. Salanne, P.A. Madden, Polarization effects in ionic solids and melts, Mol. Phys. 109 (2011) 2299–2315.
- [27] J.-B. Liu, X. Chen, J.-B. Lu, H.-Q. Cui, J. Li, Polarizable force field parameterization and theoretical simulations of ThCl4–LiCl molten salts, J. Comput. Chem. 39 (2018) 2432–2438.
- [28] G. Pireddu, A. Salcedo, H. Sauzet, S. Delpech, D. Lambertin, T. Kooyman, Polarizable force fields for the structural and thermophysical properties of molten actinide chlorides, J. Nucl. Mater. (2025) 155822.
- [29] D.J. Evans, B.L. Holian, The nose–Hoover thermostat, J. Chem. Phys. 83 (1985) 4069–4074.
- [30] Y. Ishii, S. Kasai, M. Salanne, N. Ohtori, Transport coefficients and the Stokes–Einstein relation in molten alkali halides with polarisable ion model, Mol. Phys. 113 (2015) 2442–2450.
- [31] L. Dewan, Molecular Dynamics Simulation and Topological Analysis of the Network Structure of Actinide-Bearing Materials (Ph.D. thesis), Massachusetts Institute of Technology, 2013.
- [32] H. Lukas, S.G. Fries, B. Sundman, Computational Thermodynamics: the Calphad Method, Cambridge university press, 2007.
- [33] C.W. Bale, E. Bélisle, P. Chartrand, S.A. Decterov, G. Eriksson, A.E. Gheribi, K. Hack, I.-H. Jung, Y.-B. Kang, J. Melançon, et al, Factsage thermochemical software and databases, 2010–2016, Calphad 55 (2016) 1–19.
- [34] V.P. Glushko, L. Gurvich, Thermodynamic properties of individual substances: volume 1, parts 1 and 2, (1988).
- [35] M. Rand, F.J. Mompean, J. Perrone, M. Illemassène, Chemical Thermodynamics of thorium, (no Title) (2008).
- [36] E. Capelli, R.J.M. Konings, Halides of the actinides and fission products relevant for molten salt reactors, in: Reference Module in Materials Science and Materials Engineering, Elsevier, 2020, https://doi.org/10.1016/B978-0-12-803581-8.11794-1
- [37] J. Leitner, P. Voňka, D. Sedmidubsky, P. Svoboda, Application of Neumann-Kopp rule for the estimation of heat capacity of mixed oxides, Thermochim. Acta 497 (2010) 7–13.
- [38] I. Barin, O. Knacke, O. Kubaschewski, Thermochemical Properties of Inorganic Substances, Springer-Verlag Berlin Heidelberg GmbH, 1977.
- [39] J. Chase, M. W, Nist-Janaf Thermochemical Tables, Journal of Physical and Chemical Reference Data, Monograph 9, 4 Ed., American Institute of Physics and American Chemical Society for the National Institute of Standards and Technology, Gaithersburg, MD, 1998.
- [40] A.D. Pelton, P. Chartrand, G. Eriksson, The modified quasi-chemical model: part iv. Two-sublattice quadruplet approximation, Metall. Mater. Trans. A 32 (2001) 1409–1416.
- [41] A. Smith, Structure-property relationships in actinide containing molten salts, a review: understanding and modelling the Chemistry of nuclear fuel salts, J. Mol. Liq. 360 (2022) 119426.
- [42] G.M. Photiadis, G.N. Papatheodorou, Co-ordination of thorium (IV) in molten alkalimetal chlorides and the structure of liquid and glassy thorium (IV) chloride, J. Chem. Soc., Dalton Trans. (1999) 3541–3548.
- [43] G. Wang, B. Li, P. Yang, D.A. Andersson, Ab-initio molecular dynamics simulations of binary NaCl-ThCl₄ and ternary NaCl-ThCl₄-UCl₃ molten salts, J. Mol. Liq. 385 (2023) 122347.
- [44] K. Goloviznina, M.-C. Notarangelo, J. Tranchida, E. Bourasseau, M. Salanne, Dft-based polarizable ion models for molten rare-earth chlorides: from lanthanum to europium, J. Phys. Chem. B (2025).
- [45] A. Kirshenbaum, J. Cahill, The density of molten thorium and uranium tetrafluorides, J. Inorg. Nucl. Chem. 19 (1961) 65–68.
- [46] M.H. Rand, Thorium: Physico-Chemical Properties of Its Compounds and Alloys, vol. 5, International Atomic Energy Agency, 1975.
- [47] D. Andersson, B.W. Beeler, Ab initio molecular dynamics (AIMD) simulations of NaCl, UCl₃ and NaCl-UCl₃ molten salts, J. Nucl. Mater. 568 (2022) 153836.
 [48] M. Popov, G. Gal'chenko, M. Senin, Specific heats and heats of fusion of UCl₄
- and UI₄ and heat of transformation of UI₄, Russ. J. Inorg. Chem. 4 (1959) 560–562.
- [49] A. Tosolin, E. Capelli, R. Konings, L. Luzzi, O. Beneš, Isobaric heat capacity of solid and liquid thorium tetrafluoride, J. Chem. Eng. Data 64 (2019) 3945–3950.
- [50] J. Ocádiz-Flores, A.E. Gheribi, J. Vlieland, D. De Haas, K. Dardenne, J. Rothe, R. Konings, A. Smith, Examination of the short-range structure of molten salts: ThF₄, UF₄, and related alkali actinide fluoride systems, Phys. Chem. Chem. Phys. 23 (2021) 11091–11103.
- [51] B. Li, S. Dai, D. Jiang, First-principles molecular dynamics simulations of UCl_n-NaCl (n = 3, 4) molten salts, ACS Appl. Energy Mater. 2 (2019) 2122–2128.
- [52] V. Desyatnik, S. Katyshev, Volumetric and surface properties of the NaCl-UCl₃-UCl₄ melts, Zh. Fiz. Khim. 54 (1980) 1606–1610.

- [53] Z. Singh, R. Prasad, V. Venugopal, K. Roy, D. Sood, Thermodynamics of the vaporisation of thorium tetrachloride, J. Chem. Thermodyn. 11 (1979) 31–36.
- [54] Z. Singh, R. Prasad, V. Venugopal, D. Sood, The vaporization Thermodynamics of uranium tetrachloride, J. Chem. Thermodyn. 10 (1978) 129–134.
- [55] S. Tanii, Phase diagrams of the systems thorium chloride-alkali chlorides, Denki Kagaku Oyobi Kogyo Butsuri Kagaku 32 (1964) 167–170.
- [56] A. Vokhmyakov, V. Desyatnik, N. Kurbatov, Interaction of thorium tetrachloride with chlorides of the alkali metals, Sov. At. Energy 35 (1973) 1122–1123.
- [57] R. Oyamada, Phase diagrams of ThCl₄ systems containing NaCl, KCl and LiCl and the limitation of the congruently melting compounds formation, Denki Kagaku Oyobi Kogyo Butsuri Kagaku 39 (1971) 2–5.
- [58] A. Bogacz, W. Trzebiatowski, Thermodynamic characteristics of uranium (IV) chloride in melts with alkali chlorides based on phase diagrams, Rocz. Chem. 38 (1964).
- [59] T. Kuroda, T. Suzuki, The equilibrium state diagrams of UCl4-NaCl, UCl4-KCl, UCl4-CaCl₂ and UCl4-BaCl2 systems, J. Electrochem. Soc. Jpn. 26 (1958) E140–E141.
- [60] R.E. Thoma, Phase Diagrams of Nuclear Reactor Materials, Oak Ridge National Laboratory, 1962.
- [61] N.T.H.T. Veer, S. Couweleers, J. Vlieland, J.A.O. Flores, E.F. Bazarkina, C. Hennig, L. Amidani, K. Kvashnina, R.J.M. Konings, A.L. Smith, To be decided (2025. In preparation.
- [62] N. Martynova, Z. Kudryashova, I. Vasil'kova, Enthalpy of formation of K2UCl6, KUCl5, Na2UCl6, and KNaUCl6, Sov. At. Energy 25 (1968) 1000–1001.

- [63] W. Fischer, R. Gewehr, H. Wingchen, Über thermische eigenschaften von halogeniden. 12. über eine neue anordnung zur dampfdruckmessung und über die schmelzpunkte und sättigungsdrucke von skandium-, thorium-und hafniumhalogeniden, Z. Anorg. Allg. Chem. 242 (1939) 161–187.
- [64] K.-F. Yen, S.-C. Li, G.I. Novikov, Thermodynamics of the vaporisation of thorium tetrachloride, Russ. J. Inorg. Chem. 8 (1963) 44–47. Originally published in Zhurnal Neorganicheskoi Khimii, 1963, Vol. 8, pp. 54-58.
- [65] M.-T. Su, G.I. Novikov, Thermodynamics of the vaporization of thorium tetrachloride, Russ. J. Inorg. Chem. 11 (1966) 270–273. Originally published in Zhurnal Neorganicheskoi Khimii, 1966, Vol. 11, pp. 318-322.
- [66] M.E. Mueller, The Vapor Pressure of Uranium Halides, Technical Report, Originating Research Org. not identified, 1948, https://doi.org/10.2172/4440808. https:// www.osti.gov/biblio/4440808
- [67] J.J. Katz, E.E. Rabinowitch, Chemistry of Uranium. Collected Papers, Technical Report, Argonne National Lab., Lemont, Ill., 1958, https://doi.org/10.2172/ 4261677. https://www.osti.gov/biblio/4261677
- [68] K. Sawlewicz, S. Siekierski, Determination of the vapour pressure of uranium tetrachloride by the gas saturation method, Radiochem. Radioanal. Lett. 23 (1975) 71–77
- [69] M. Smirnov, V.Y. Kudyakov, The saturation vapour pressure and decomposition potential of ThCl4 solutions in molten alkali chlorides, Electrochim. Acta 29 (1984) 63–68.